AIP | Applied Physics Letters

Conductor microstructures by laser curing of printed gold nanoparticle ink

Jaewon Chung, Seunghwan Ko, Nicole R. Bieri, Costas P. Grigoropoulos, and Dimos Poulikakos

Citation: Appl. Phys. Lett. **84**, 801 (2004); doi: 10.1063/1.1644907
View online: http://dx.doi.org/10.1063/1.1644907
View Table of Contents: http://apl.aip.org/resource/1/APPLAB/v84/i5
Published by the American Institute of Physics.

Conductor microstructures by laser curing of printed gold nanoparticle ink

Jaewon Chung, Seunghwan Ko, Nicole R. Bieri,[a] Costas P. Grigoropoulos,[b] and Dimos Poulikakos[a]
Department of Mechanical Engineering, University of California, Berkeley, California 94720-1740

(Received 2 September 2003; accepted 5 December 2003)

The laser-based curing of printed nanoparticle ink to create microlines (resistors) of electrical resistivity approaching that of bulk gold was investigated. The present work relies on laser absorption in both the nanoparticle ink and the sintered gold layer, as well as the transport of thermal energy in the substrate and the resulting solvent vaporization and nanoparticle deposition and sintering. The morphology and electrical properties of the gold line can be controlled by modulating the spatial distribution of the laser beam intensity. Based on the understanding of the underlying physics, a process that circumvents a serious drawback on the functionality of cured gold microlines is produced. Microconductors with resistivity approaching that of bulk gold are produced, while loss of gold nanoparticles and cross sectional nonuniformities are avoided. © *2004 American Institute of Physics.* [DOI: 10.1063/1.1644907]

The emergence of consistent manufacturing methods of ultrafine particles (UFP) of a host of materials is creating a vivid activity related to the utilization of these particles. Thermophysical properties significantly different from those of bulk counterparts can be realized in future-oriented engineering applications. Specific to this work, gold nanosized particles under 5 nm in diameter possess lower melting temperature (~300–500 °C) compared to the melting temperature of bulk gold (1063 °C),[1] which enables fabrication of electrical conductor lines on the substrate. The need-driven trend in electronics manufacturing is to develop constantly smaller and tighter packed components. There are also areas where cost effectiveness and rapid processing are more critical than ultrasmall feature size, such as the fabrication of flat panel displays using doped polymers, electronic cards, etc. Corresponding to these requirements, direct writing (additive) processing using jet printing technology has gained significant interest as an alternative approach to conventional, subtractive integrated circuit (IC) processes.[2–5]

In the previous work,[6] the resistivity of the produced microlines was markedly higher than that of bulk gold. As a result, while the curing of the printed lines was definitively demonstrated, the utilization of these lines as electrical conductors remained questionable. In addition, the physical phenomena of the process were only partially explored. Fine lines of nanoparticle ink were created on a glass substrate by the generation of nanoparticle ink microdroplets using a modified drop-on-demand (DOD) printing.[6] After generating stable droplets of 46 μm diameter (i.e., 51 pL) at 30 Hz, a continuous line was made on the glass substrate by moving a precision translation stage at 2 mm/s. The width of the printed line was measured at about 125 μm. Therefore, the cross sectional area of the ink lines before curing is about 765 μm^2, correspondingly. The ink is composed of 2–4 nm size gold particles (30%–35% weight, 1.9%–2.3% volume)[7] in toluene. Consequently, the expected maximum cross-sectional area of a gold line would be 14.5–17.6 μm^2 assuming that all toluene evaporates and all gold nanoparticles are fully melted to form a pore-less layer possessing bulk gold properties. The resulting resistance per length is calculated as 1.26–1.52 Ω/mm using the resistivity of bulk gold. Following the printing, an argon laser beam at the wavelength of 514 nm (Ref. 8) was applied at the center of a printed line with 45° of incidence angle.

Atomic force microscope (AFM) images in Fig. 1(a) depict the morphology of laser cured gold line at 100 mW of incident laser power and 0.2 mm/s of translation speed. This morphology resembles a ''volcano'' cross section. Figure 1(b) shows an *in situ* micrograph of the laser curing process. The beam waist ($1/e^2$) along the minor axis that is perpendicular to the printed line is 27 μm and the beam waist along the major axis is 38 μm. A highly reflective gold layer begins to form near the evaporation interface contact line. The toluene evaporates due to laser radiation absorption in the sintered gold layer and the subsequent thermal diffusion toward the evaporation interface. Due to thermocapillarity, ink was displaced ahead and around the scanning laser spot forming a U-shaped convex ink meniscus. Gold nanoparticles are mainly deposited right at the evaporation interface contact line. Neglecting thermal losses due to radiation, convection and evaporation, the calculated temperature profiles of the substrate induced by scanning a continuous Gaussian elliptic laser beam[9] were employed to provide approximate quantitative information on the temperature field. The isotherms in Fig. 1(b) show that the region bounded by the evaporation interface contact line is only slightly narrower than the isotherm at 110 °C which is the evaporation temperature of toluene under atmospheric pressure. Guided by experimentally observed interface contours, the shape of the evaporation interface contact line is modeled as semicircular, following the isotherm profile. It was assumed that the gold nanoparticles are approximately deposited at the same speed at the semicircular evaporation interface contact line. Since the arc

[a]Also at: Laboratory of Thermodynamics in Emerging Technologies, Department of Mechanical and Process Engineering, ETH Zurich, CH-8092 Zurich, Switzerland.
[b]Author to whom correspondence should be addressed; electronic mail: cgrigoro@me.berkeley.edu

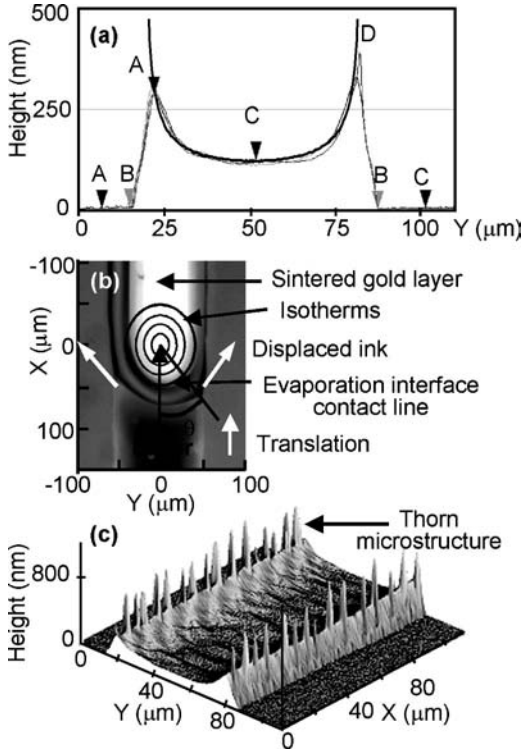

FIG. 1. Single laser cured gold line at 100 mW of incident laser power at 0.2 mm/s of translation speed: (a) AFM cross-sectional profiles. The vertical distances of A and C points is 283.6 and 121.34 nm, respectively, and the horizontal distance of B points 72.6 μm. Profile D is the curve fit by Eq. (1); (b) *in situ* reflection image of laser curing process of NPS (top view) and calculated isotherms. Temperatures of the isotherms are 110, 150, 200, and 250 °C from outside to inside; (c) AFM three-dimensional surface plot.

length of the evaporation interface contact line corresponding to the increment, Δy is $\Delta y/\cos\theta$ [Fig. 1(b)], the topography of the deposited gold along the y-axis $[t(y)]$ can be obtained as

$$t(y)=\frac{t(0)}{\cos\left[\sin^{-1}\left(\frac{2y}{W}\right)\right]}\quad\left(\text{when}\quad |y|<\frac{W}{2}\right),\tag{1}$$

where $t(0)$ is the thickness of the deposited gold at the center of the line ($y=0$) and W is the width of the gold line which is equal to the distance between the center of the laser beam and the evaporation interface contact point. The theoretical profile D matches very well the AFM image [Fig. 1(a)]. An interesting finding, better visualized in the three-dimensional AFM picture of Fig. 1(c) is that for the "low" curing power of 100 mW, thorn microstructures with height in the range between 500 and 1000 nm were formed at the rim of the line, spaced with a period of about 8 μm. They were formed only when nanoparticle ink was displaced around the area heated by the laser beam [Fig. 1(b)]. The convex ink meniscus [Fig. 1(b)] formed due to both thermocapillary flow and the evaporation near the laser spot, features an azimuthal instability (i.e., it is unstable in the direction along the ridge of the U-shaped convex ink meniscus) because of the high thermal Marangoni number that is calculated as 400–1000.[10] To this end, convection microcells were formed in the displaced ink delivering particles that are cured at the locations of the curing line where the thorn microstructures appear. A related instability in thermocapillary flows was discussed by Skotheim *et al.*,[11] Sharma *et al.*,[12] and Stowell *et al.*[13] In addition, it is noted that these thorn microstructures survived after reirradiation by high laser intensity, thereby eliminating the possibility of internal voids.

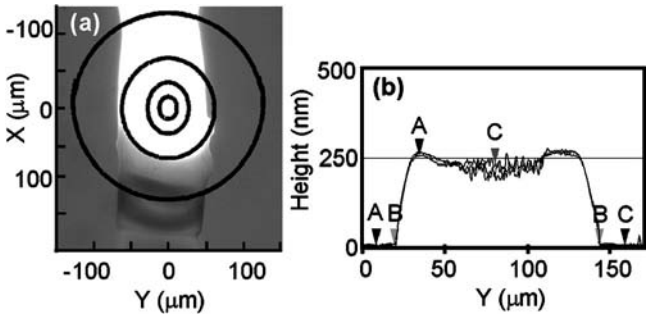

FIG. 2. Single laser cured gold lines at 300 mW of incident laser power and 0.2 mm/s of translation speed. (a) *In situ* reflection image of laser curing process of NPS (top view) and calculated isotherms. Temperatures of the isotherms are 110, 200, 400, and 600 °C from outside to inside; (b) AFM cross-sectional profiles. The vertical elevation distances of the A and C points are 256.4 and 248.1 nm, respectively and the horizontal distance separating the B points 123.1 μm.

When the laser power increases to 300 mW at 0.2 mm/s of translation speed, the deposited suspension was not displaced around the scanning laser spot. This different behavior is directly related to the markedly smaller curvature of the 110 °C isotherm in Fig. 2(a) compared to Fig. 1(b). Accordingly, the topography of the deposited gold line is flatter [Fig. 2(b)] and the train of thorn microstructures did not form. At the center region of the gold line in Fig. 2(b), the temperature was elevated above 400 °C according to calculated isotherms in Fig. 2(a) and the surface morphology became rougher due to full melting of the sintered film and capillary-induced agglomeration.

Figure 3 shows the resistance per length of gold microlines cured by single laser beam. As the laser power increases and the scanning speed decreases, the resistance per unit length decreases due to more complete curing. At 500 mW and 0.2 mm/s, the resistance per unit length is 4.2 Ω/mm which is about 3 times the value obtained when the resistivity of bulk gold and 14.5–17.6 μm^2 of cross sectional area (as noted previously, this assumes full sintering of all nanoparticles in the printed line) are used.

Considerable insight into the physical mechanisms of the laser curing process was achieved using the single Gaussian

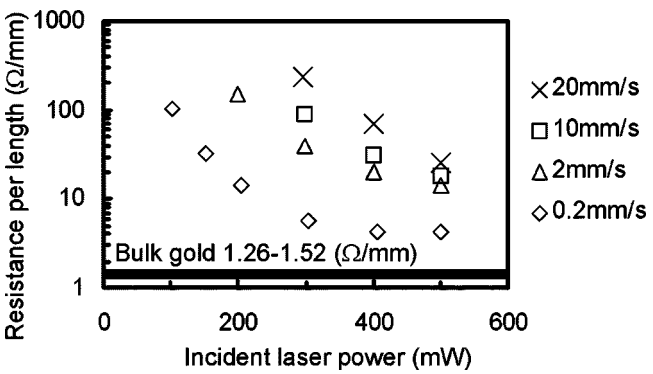

FIG. 3. Resistance per unit length of single laser cured gold lines at different incident laser powers.

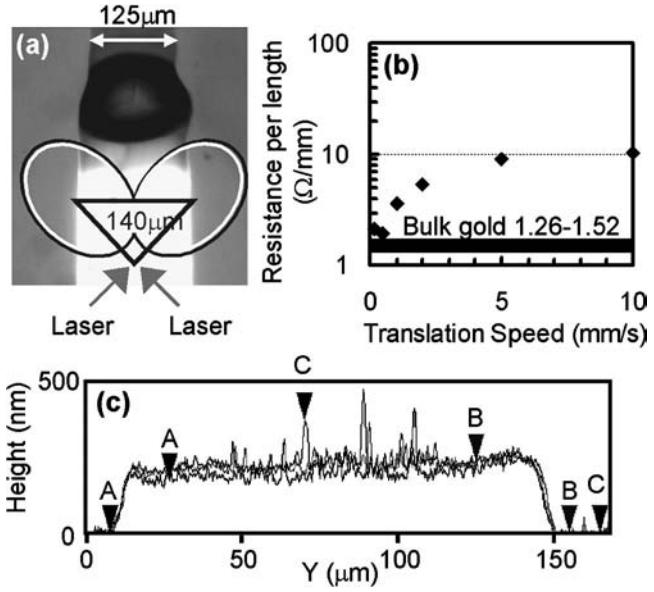

FIG. 4. Results of functionalized double laser cured gold lines. The beam waist $(1/e^2)$ of each laser is 28.5 μm and incident laser power is 603 mW (1206 mW in total): (a) *in situ* reflection image of laser curing process of NPS (top view); (b) resistance per unit length vs translation speed; (c) cross-sectional profiles of AFM image at 0.5 mm/s of the translation speed. The vertical elevation distances of A, B, and C points are 180, 240, and 377 nm, respectively. The average cross-sectional area is 28.5 μm^2.

laser beam for processing. However, the original technical goal of achieving lines of resistivity neighboring that of bulk gold was not reached, because of limitations imposed by the interplay of the physical mechanisms involved. In many cases, a portion of the nanoparticle ink was displaced to the sides due to thermocapillarity. This displaced uncured ink was washed away in an extra step and wasted. Furthermore, the single laser beam, for reasons explained earlier, tends to generate elevated rims with the train of thorn microstructures that are suboptimal in resistors. A properly modulated shape of the laser beam accounting for the physics discussed above while maintaining process simplicity, can lead to nearly bulk electrical resistivity and alleviate the problem of wasted uncured ink. This was achieved by dividing the laser beam through a beam splitter and focusing using two respective lenses, thus achieving a ''heart'' shape energy input on the deposited ink line. In the particular example of Fig. 4, the focal waist $(1/e^2)$ of each laser beam was 28.5 μm. Since the incidence angle of the laser beams was 45°, the beam waist along the minor axis was 28.5 μm and that of the major axis 40.5 μm. The incidence plane is aligned to the printed line at 45° from both left and right. The distance between the centers of the laser spots is set at 140 μm, which is larger than the width of the printed line, aiming to guide the ink by thermocapillarity toward the center of the line, thus minimizing material loss. The *in situ* image of double laser curing process at 603 mW of laser beam power (1206 mW in total) and 0.5 mm/s in Fig. 4(a) shows that this strategy indeed works. AFM image in Fig. 4(c) displays the cross sectional profile of a cured gold line with this ''heart'' laser irradiance distribution. The thickness of the cured line was about 200 nm. In addition, the morphology is almost flat due to the slightly bent evaporation interface contact line that is shown in Fig. 4(a). The resistance per unit length of the lines sintered on substrates moving with different translation speeds is shown in Fig. 4(b). At low translation speeds, the data approach the resistance per length value of bulk gold. As the translation speed increases, the gold line experiences lower temperature during a shorter transient heating time. This results in the increase of the resistance per length. Further tailoring to specific applications is a matter of parametric optimization and not of interest to this report.

In closing, we reported reduced temperature, nanoparticle based conductor microstructuring. The involved physics lies at the intersection of nanoparticle phase change (melting) in the presence of an evaporating carrier liquid, monochromatic radiation absorption by the nanoparticles and free surface thermofluidics. Understanding of these phenomena and their effect on the morphology and resistance of the cured microstructure led to application of a ''heart'' shaped laser beam, with which the feasibility of fabricating conductor lines of resistance per length neighboring that of bulk gold was demonstrated.

Partial financial support to the University of California, Berkeley by the DOE under Grant No. DE-FG03-95ER14562 and to the Swiss Federal Institute of Technology in Zurich by the Swiss National Science Foundation under Grant No. 2000-063580.00 is gratefully acknowledged.

[1] P. A. Buffat and J. P. Borel, Phys. Rev. A **13**, 2287 (1976).
[2] S. B. Fuller, E. J. Wilhelm, and J. M. Jacobson, J. MEMS **11**, 54 (2002).
[3] J. B. Szczech, C. M. Megaridis, D. R. Gamota, and J. Zhang, IEEE Trans. Electron. Packaging Manufacturing **25**, 26 (2002).
[4] J. Bharathan and Y. Yang, Appl. Phys. Lett. **72**, 2660 (1998).
[5] T. R. Hebner, C. C. Wu, D. Marcy, M. H. Lu, and J. C. Sturm, Appl. Phys. Lett. **72**, 519 (1998).
[6] N. R. Bieri, J. Chung, S. E. Haferl, D. Poulikakos, and C. P. Grigoropoulos, Appl. Phys. Lett. **82**, 3529 (2003).
[7] The original gold weight concentration in toluene gold nanoparticle solution was 30%. However, due to the evaporation of the toluene in the reservoir of the jetting head, the gold weight concentration increased up to about 34(±1)% during the operation of the jetting. Therefore, 30%–35% of the gold weight concentration was used for the calculation.
[8] To prevent the direct heating of laser on the transparent substrate, the laser at the visible wavelength was selected. In addition, due to the small absorption depth of the nanoparticle ink on the wavelength of the incoming laser radiation (Ref. 6), when the laser is directly irradiated to the printed ink, most of the radiation will be absorbed in the close vicinity of the free surface of printed line.
[9] J. E. Moody and R. H. Hendel, J. Appl. Phys. **53**, 4364 (1982).
[10] Marangoni number for Fig. 1(b) was calculated from

$$\mathrm{Ma} = \gamma \frac{\Delta T}{L} \frac{H^2}{\mu \alpha}$$

where γ, μ, and α are the thermal gradient of surface tension, viscosity and thermal diffusivity of pure toluene, respectively. The width of the displaced U-shaped ink [Fig. 1(b)] was used for L and the difference between the evaporation temperature of toluene and the room temperature was used for ΔT. The value of 5–10 μm was used for H.
[11] J. M. Stotheim, U. Thiele, and B. Scheid, J. Fluid Mech. **475**, 1 (2003).
[12] A. Sharma and G. Reiter, J. Colloid Interface Sci. **178**, 383 (1996).
[13] C. Stowell and B. A. Korgel, Nano Lett. **1**, 595 (2001).